ELSEVIER

PII: S0011-2275(98)00010-1

Cryogenics **38** (1998) 525–531

Printed in Great Britain
0011-2275/98/$19.00

Mithrandir + : a two-channel model for thermal-hydraulic analysis of cable-in-conduit super-conductors cooled with helium I or II

R. Zanino*†, L. Bottura‡, L. Savoldi† and C. Rosso§

†Dipartimento di Energetica, Politecnico, 24 c. Duca degli Abruzzi I-10129, Torino, Italy
‡CERN, Div. LHC-MTA, CH-1211, Geneve 23, Switzerland
§CryoSoft, 5 rue de la Belette, F-01710, Thoiry, France

Mithrandir[1] – a 1-D code for the analysis of thermal-hydraulic transients in cable-in-conduit super-conductors (CICC) with cooling channel – has been extended to helium II by including Gorter-Mellink heat transport. The code treats the general case of different thermodynamic properties and flow velocities for the helium in the cable bundle region and that in the cooling channel, which are coupled to conductor and jacket at different temperatures. A detailed validation of the code against a thermal-hydraulic experiment in helium II is presented, showing good agreement, and code convergence is demonstrated numerically. We present results of simulations of the QUench Initiation and Propagation Study (QUIPS) experiment, concentrating mostly on the initial phase of the quench. We show that the simulation is at least qualitatively in agreement with experimental data.

Keywords: quench; cable in conduit conductors; super-fluid helium

Introduction

Cable-in-conduit conductors (CICC's) operated in supercritical helium at about 4.5 K, in close vicinity of the pseudo-critical line, are known to possess superior stability properties. This is mainly due to their large wetted perimeter, which allows an optimal use of the helium heat capacity as a heat sink for enthalpy stabilization.

The major drawback is that the frictional pressure drop that must be overcome to circulate the helium can become considerable, resulting in a large heat load on the refrigerator and, in the limit of large mass flows or long cable lengths, reduced cooling efficiency caused by the temperature increase during the isenthalpic expansion along the cable. A second limitation is on the maximum field that the cable can reach. Even in the case of Nb3Sn, operation at 4.5 K with a convenient cable space current density, of the order of 40 A/mm^2, is possible only up to fields of the order of 13 T. NbTi is limited to fields of the order and below 7 T.

Operation in super-fluid helium has been proposed in recent years to overcome these two limitations[2,3]. Stagnant super-fluid helium is known to possess high heat transfer capability, so that forced flow is no longer necessary to remove the heat loads on the coil, provided that the heat flux to be sustained by the fluid is below the critical upper limit q^*. In addition, the reduced operating temperature around 1.8 K results in an increase of the critical current of the superconductor. Therefore, the cable can be operated at increased field maintaining the same temperature margin. Finally, the excellent heat transport properties of super-fluid helium increase the cooling at the wetted surface of the strands. Hence the pseudo-cryostability condition results in large values of the limiting current density, that is therefore no longer a dominant term in the conductor design.

Two examples of proposed applications for CICC operated in super-fluid are the super-conducting outserts of the 45 T hybrid solenoid in construction at the National High Magnetic Field Laboratory (NHMFL)[3] and the Bechtel proposal for a cable for a large size Super-conducting Magnetic Energy Storage (SMES)[2]. In the first case the cables for the outserts are standard CICC's, i.e., a Nb3Sn cable bundle with a large void fraction, of the order of 40%, jacketed in a thick steel conduit. Operation at 1.8 K is foreseen mainly to achieve a high field, of the order of 15 T, on the high field outsert module. In the second case the 200 kA CICC has a very large cooling hole, separated by a perfor-

*To whom correspondence should be addressed.

ated wall from the NbTi cable bundle. The cross section of the hole is large, of the order of 10^3 mm^2, and is necessary for the super-fluid helium to remove the steady state heat flux from and into the cable during operation.

The main purpose of the work presented here is to extend an existing model for the analysis of CICC's with and without separate cooling hole to the case of operation in super-fluid helium. In particular we wish to be able to model the main features of heat transport related to the Gorter-Mellink mechanism, but we will not concentrate on the physics of super-fluid helium, which is a complex subject of its own.

From Mithrandir to Mithrandir + : extension of the computational model to helium II

Mithrandir[1] is a 1-D (x coordinate along the conductor) time dependent model developed as an extension of the Gandalf code[4]. It allows different thermodynamic state of the helium in the cable bundle region and the helium in the cooling channel. These two regions communicate through a wall, which is typically perforated in order to allow pressure exhaust in the case of a quench. The coupling between the two regions is controlled in the code by a set of 'free' parameters, among which the most important are: the perforation fraction F, and the multiplier H_{nowall} of the heat transfer coefficient between bundle and hole (see also below), to be applied at the perforation. The code has been recently validated for HeI against thermal-hydraulic and quench data from the QUELL experiment[5,6], and the same experiment was also analyzed from the point of view of stability[7].

The detailed set of equations implemented in Mithrandir is given in Ref. [1]; below we shall concentrate on the two major developments of the code which are relevant here, i.e., the helium II model, and the extension of the helium properties to the region below the λ point.

Helium II model

Several levels of approximation can be found in the literature on HeII thermal-hydraulics, ranging from full two-fluid models (set of 2-D PDEs for the normal and super-fluid components) to simple empirical models (single 1-D PDE). In Mithrandir + we use for the helium in each of the two regions a standard set of 1-D one-fluid equations, augmented only by the Gorter-Mellink (G-M) contribution[8]. The energy source Λ_e in the pressure and temperature equations of Ref. [1] contains therefore an additional term, corresponding to the divergence of the G-M nonlinear conductive heat flux.

In order to justify this simple approach we start observing that very recently a one-fluid model[9] has been derived under reasonable assumptions from the classical two-fluid model of Landau. The major features of the one-fluid model are that: 1) the standard continuity equation for the total (i.e., normal plus super-fluid) density stays valid; 2) the total momentum equation is modified with respect to the standard one, and includes G-M type contributions; 3) the standard energy equation is modified by the simple addition of the divergence of the G-M conductive heat flux. The G-M (temperature gradient dependent) contributions in the total momentum equation appear as: α) an additional force acting on the fluid, β) an additional contribution to the standard viscous stress. Therefore, we essentially need to justify only the neglect of the mentioned α and β terms in Mithrandir + .

It is easy to see that, when the difference between normal and super-fluid speed is of the same order of the one-fluid speed, the α term scales as the Mach number squared when compared with the pressure gradient; this means it should be negligible in the 1-D cases of interest for us where the flow is typically very subsonic. (It is worth observing that also in the examples presented in Ref. [8] the flow is subsonic, but in the 2-D situation considered there the α term gives a force which is not negligible at least in *one* of the two directions. Also, the flow in that case is dominated by natural convection, as opposed to forced convection in our case).

Concerning the β term it appears as *third* order derivatives of the temperature in the total momentum equation[8]. This type of term could not be consistently included in the linear finite element formulation used in Mithrandir + since it trivially vanishes because of the first degree interpolation used. Under the same assumption as above, the β term can be estimated to be in principle of the same order of magnitude of standard stress tensor terms. In order to assess the actual relative importance of this term, however, we computed it *a posteriori* with a finite difference approximation, together with the pressure gradient and the friction term, for two cases of relevance here. In the steady state obtained in a pure thermal-hydraulic experiment (see below), the β term turned out to be everywhere orders of magnitude smaller than both pressure gradient and friction. At the transition through the λ line in a quench simulation (see below), the same was true, both in the hole and in the bundle. This qualitatively justifies having neglected the β term here.

The friction factor f used in Mithrandir + is chosen as the maximum between the laminar[8] and the turbulent value. For the turbulent value we use: $f_T = 0.43\ (49.5/(\mathrm{Re})^{0.88} + 0.051)$ in the bundle, and $f_T = 0.092/\mathrm{Re}^{0.2}$ in the hole, where Re is the respective Reynolds number.

Different heat transfer coefficients are used for the energy exchanges between helium and strands (h_{Si}), helium and jacket (h_{Jk}), and between helium in the bundle and helium in the hole (h_{eq}, h_{HB}). For the former two we use the correlations given in Ref. [10]. For the latter, we need to distinguish between the exchanges through the wall separating hole and bundle (h_{eq}), and those directly through the perforation (h_{HB}). For the former, the conductance resulting from a series of thermal resistances is used. As to the (conductive) energy exchange through the perforation, it is modeled here as proportional to the limit of h_{eq} for vanishing wall thickness δ; because of the complexity of the phenomena actually involved, we use an arbitrary multiplier H_{nowall} leading to the following relation: $h_{HB} = H_{nowall}\, h_{eq}(\delta = 0)$.

Because of the parabolic nature of the energy equation, due to the inclusion of the G-M contribution, we impose on the helium II two conditions at each boundary. This departs from the case of helium I where, because of the convective nature of energy transport, two conditions are imposed at each inflow boundary, and only one at each outflow boundary.

Helium properties

Evaluation of the thermophysical properties of helium is a fundamental ingredient of CICC modeling. The primary

variables used in both codes are pressure p and temperature T. To increase efficiency we have generated dedicated tables of the required properties, taking as a reference source the HEPAK package[11]. The tables contain the smallest possible number of pressure and temperature couples, distributed in a nonuniform grid, needed to interpolate the properties up to a typical accuracy of 3%.

The interpolation grid (i,j) consists of lines at constant pressure p_i where the grid points are placed, unevenly spaced, at temperature $T_{i,j}$. The grid generation and interpolation is done taking a slice of the property surface at constant pressure p_i. Grid points $T_{i,j}$ are placed adaptively along the temperature axis to achieve an accuracy set to half of the total error contingent (i.e., 1% to 2%). The next slice at constant pressure p_{i+1} is then generated using the same method. The total interpolation error is estimated scanning the space (p,T) bracketed by the two pressure slices p_i and p_{i+1}, taking the linearly interpolated values at temperature T along both slices, and linearly interpolating in pressure. The slice at pressure p_{i+1} is finally moved adaptively to achieve the global accuracy goal.

The same method is used for the interpolation of properties at any given point (p,T). The table is searched first along the pressure axis, to determine the p_i and p_{i+1} lines bracketing the point. Linear interpolation is used on each constant pressure line, to calculate the value at the desired temperature T, followed by a linear interpolation in pressure.

The domain of validity is for pressure between 10^3 Pa and 10^8 Pa, while for temperature between 0.8 K and 1000 K, of course avoiding the melting region. In the close vicinity of the saturation, melting and λ lines some of the properties are divergent, and the error check described above fails. Therefore, within a band of 0.1 K around the saturation and λ lines, in a rectangular box of 0.1 K and 0.25 bar around the critical point, and within a band of 2.0 K below the melting line the error control is ignored, and the interpolation uses a fixed step in temperature of 0.1 K. In this case, the interpolated values are rearranged to manage the discontinuities or divergence of the thermophysical properties, using a one-sided extrapolation.

Not the whole region above has been mapped by grid points. At high temperature we used fits to boost speed and decrease memory requirements. The Gruneisen parameter has been fitted above 130 K, the viscosity above 50 K and the thermal conductivity above 100 K. In addition a perfect gas region has been determined, namely where the density deviates from the perfect gas value by less than 1%. In this region the perfect gas asymptotic limit is returned. In two cases, for Cp and viscosity, we needed simplified perfect gas fits to improve the accuracy and thus satisfy the total accuracy requirements. The super-fluid thermal conductivity function is a special case, where a fit has been used instead of interpolation. The fit error is of the order of 8% of the maximum value. We judged this accuracy to be enough, based on the large uncertainty in the measured values quoted in the literature.

Code validation and convergence analysis for a thermal-hydraulic experiment

Simulations with Mithrandir + have been performed to validate the code against experimental data produced by Srinivasan and Hoffman[12]. Using thermometers with a ± 3 mK accuracy, they measured the HeII temperature profiles and critical heat flux in a stainless steel tube (0.8 m long) filled with stagnant or flowing subcooled He II, with a resistive heater supplying a constant power to the conduit.

In order to simulate this set of experiments, we treat the tube as a degenerate case of a CICC with cooling channel, assuming vanishing (i.e., reduced by several orders of magnitude) bundle cross section; we then set to zero the value of the perforation between bundle and hole; finally, heat transfer between helium in the hole and helium in the bundle is not allowed. This is obviously not the best situation for a validation of Mithrandir + , still it was chosen because of lack of thermal-hydraulic data referring to HeII in CICCs with cooling channel. The very good agreement which results (see below) shows on the other hand the robustness of the code when applied to a topologically extreme condition.

In the case of stagnant HeII, constant p and T at inlet and outlet are imposed, with an initial linear temperature profile. In the case of flowing He II, p and T at inlet and T at outlet are imposed as boundary conditions, while p at outlet is computed from the given constant mass flow rate. We adopt a uniform mesh along the tube, and the heater is treated as a uniform heat source placed at the middle of it. The transient is followed for 100 seconds with an adaptive mesh. Steady state is reached in O(10)seconds.

Figure 1 shows the results of the simulation in a no flow case. For relatively coarse meshes the number of nodes that are located on the heater (0.02 m long) is too small, so that it cannot be resolved properly. However, provided spatial convergence is reached, the choice of simulated heater length does not influence the very good agreement with the experimental data. Comparable agreement for this case was also obtained with simpler models[13].

Effect of Gorter-Mellink heat conduction

We have analyzed a similar type of transient, this time in presence of a background flow.

Here the heater is modeled as a 0.1 m source, so that 400 nodes are enough to have a good agreement with the

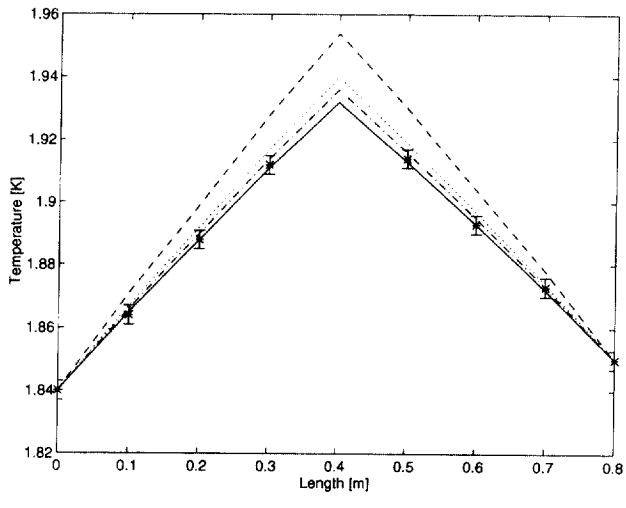

Figure 1 Simulation with W = 0 g/s, p = 1 bar, input power Q = 0.205 W. Uniform mesh with: 400 nodes (dashed), 800 nodes (dotted), 1200 nodes (dash-dotted), 2000 nodes (solid). Experimental data are indicated by symbols (*) with the respective error bars

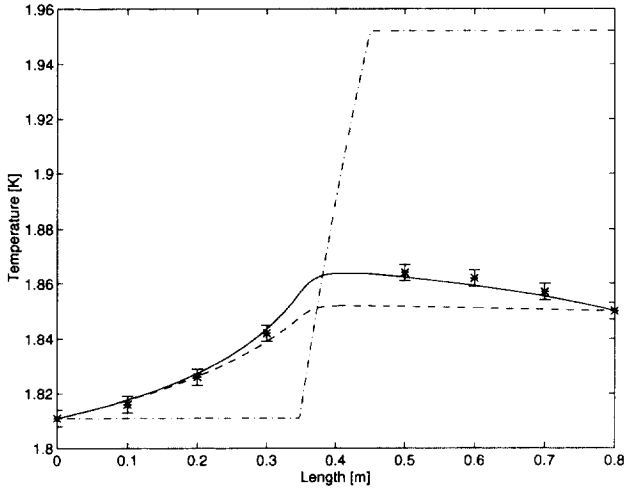

Figure 2 Simulation with W = 0.319 g/s, p = 2.5 bar, input power Q = 0.169 W. Exponent m = 3 in the G-M term (solid), exponent m = 3.4 in the G-M term (dashed), vanishing G-M term (dash-dotted). Experimental data are indicated by symbols (*) with the respective error bars

experimental points (*Figure 2*). For this case about 3/4 of the total input power is removed by G-M conduction; in fact, the results obtained in the absence of the G-M term completely disagree with the experiment. One also notices from *Figure 2* that the effect of the exponent[8] in the G-M term is not very important in this case.

Critical heat flux

The minimum heat power Q_0^* leading to a transition of HeII to HeI has been computed in the case of stagnant helium, for different bath temperatures T_{bath}. The corresponding critical heat flux through each half of the tube is defined as $q^* = Q_0^*/2A_{TS}$, where A_{TS} is the test cross section. Computed and experimental results for the critical heat flux are reported in *Figure 3* in the conventional form giving $q^* L^{1/3}$ (L is half of the tube length) as a function of T_{bath}. There is very good agreement between experiment and simulation, even if the temperature excursion is now transient and larger than in the previous Figures.

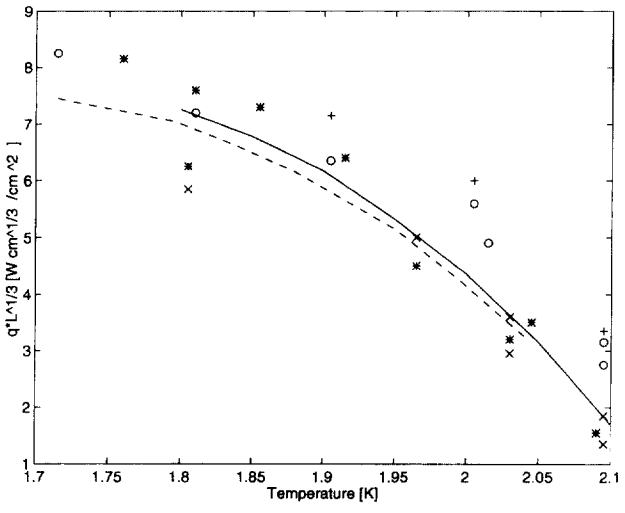

Figure 3 Scaled critical heat flux as a function of bath temperature. Mithrandir + simulation (solid line), experiment [10] (dashed line), other experimental data taken from Ref. [10] (symbols)

Analysis of space and time convergence

The spatial convergence of the code at steady state has been checked by monitoring the relative energy conservation error E as a function of the number of nodes. As expected for finite elements using linear test and trial functions, E decreases proportionally to the number of nodes (*Figure 4*a).

The time convergence of the code has been investigated by running it with different (nonadaptive) Δt in the range $10^{-4} \div 10^{-1}$ s, using a fully implicit method. The relative errors plotted in *Figure 4*b are computed at t = 1 s, using as reference solution the one obtained with $\Delta t = 10^{-4}$ s. As expected for a first order time marching scheme, the error decreases proportionally to the time step.

Quench modeling for the QUIPS experiment

We have simulated the QUench Initiation and Propagation Study (QUIPS) experiment[14] with Mithrandir + . The experiment, designed and executed in a joint effort by Bechtel and NHMFL in order to study stability and quench in HeII, was performed at NHMFL on a sub-scale version of the Bechtel CICC for SMES applications[12]. The test cable has an 'inside-out' topology (*Figure 5*) if compared to a CICC with central cooling channel: the cable bundle is inserted into a perforated pipe, placed centrally inside an unperforated conduit. The free annular space between the two represents the 'hole'. The 67 m long conductor, closed at one end (x = 0), is wound in a two-layer coil.

The nominal perforated fraction of the pipe separating bundle and hole is F = 0.001. It must be emphasized, however, that the actual value of F is not known precisely. F will be equal to or smaller than its nominal value, because the cables can occlude part of the perforation.

At the beginning of the transient the He II is at atmospheric pressure (we neglect the hydrostatic head, $\leq$ 1 m) and 1.8 K. In the simulation p and T are imposed at the open end, while at the closed end the flow velocity vanishes.

In the experiment, quenches are obtained at 6 kA and 8 kA; unless otherwise noticed, we shall restrict our analy-

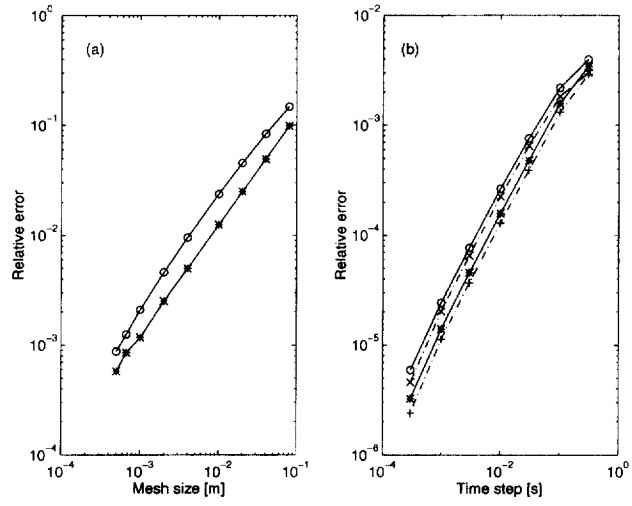

Figure 4 (a) Spatial convergence of Mithrandir + . Relative energy conservation error with a uniform heat pulse: W = 0 g/s (*), W = 0.319 g/s (o). (b) Time convergence of Mithrandir + : W = 0 g/s (o = ∞-norm; x = 2-norm), W = 0.319 g/s (* = ∞-norm; + = 2-norm)

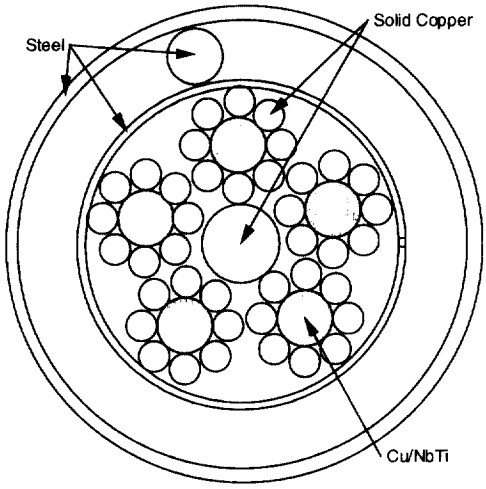

Figure 5 Cross section of the QUIPS conductor (Courtesy of J.R. Miller)

sis to the former case. At 6 kA the average (self) magnetic field on the conductor is estimated to be about 0.22 T. A 0.1 m long inductive heater is located at the closed end, supplying power which decays exponentially with a time constant of ~ 0.7 ms. We assume, unless otherwise noticed, that the whole power is deposited into the strands, uniformly over the heater length. For typical input power per unit length of ~ 50 kW/m at t = 0, the quench starts 'instantaneously' in the simulation, with an initial normal zone equal to the heater length.

Initial stage of the quench

Let us consider first a typical evolution of He pressure and temperature at a given location in the normal zone, in a case with finite perforation (nominal F). In *Figure 6*a we show the evolution of the pressure in bundle and hole, near the heater end, while in *Figure 6*c we report the corresponding thermodynamic trajectory in a (p,T) diagram for the He at the same location.

The helium in the bundle is heated by the normal conductor and it depressurizes because of its negative bulk thermal expansivity[8] below the λ transition. This causes an instantaneous mass flow from the hole, and a backwards flow from the end of the normal region after a time of the order of heater length/sound speed (first knee in *Figure 6*a,c). At the transition to HeI, corresponding to a temperature of ~2.2 K, the expansivity changes sign and this causes the sharp pressure increase at t = 2.5 ms (second knee in *Figure 6*a,c).

The initial depressurization of the He in the hole (due to the mass flowing *to* the depressurizing bundle) is followed by a fast pressure increase (due to the mass flowing *from* the pressurizing bundle). The hole pressure increases quasi adiabatically because the He mass transfer to account for the pressure increase is small, and the thermal conduction through the wall occurs on a time scale, which is much longer than that examined here. The He in the hole evolves therefore almost isentropically, and, notwithstanding the significant pressurization, the variation of its temperature is negligible because of the proximity of the isobars in this thermodynamic region.

As we see from *Figure 6*c, the He in the bundle follows a thermodynamic trajectory that eventually hits the saturation line (dashed line), indicating that boiling takes place in this case. For the nominal value of F this happens at t ~ 15ms. Our model, however, considers He as a single-phase fluid. Therefore, it is unfortunately not suited to accurately follow the transient in the liquid-vapor region.

It is instructive to follow the same evolution as above in the limiting case where we take F = 0 (i.e., vanishing perforation between hole and bundle). The results of this case are reported in *Figure 6*b,d. One can notice that the helium in the bundle is quickly pressurized to supercritical conditions. The helium in the hole is essentially unperturbed, because conductive heat transfer through the wall is the only coupling mechanism left between bundle and hole, and it is very slow (compared to sound time scales) as already mentioned.

Because of the uncertainty on the actual value of F[5,6], it is meaningful to consider parametrically the effect of different perforations on, e.g., the boiling onset time τ_B. In *Figure 7* we report τ_B as a function of F. The simulations show that the helium starts boiling in ~ 10 ms, for most values of F considered here, except for extremely small $F \leq 10^{-5}$. A second uncertainty in the model is the thermal coupling

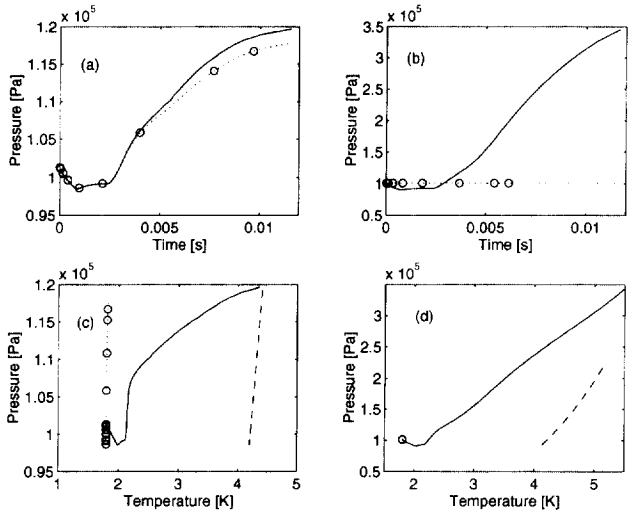

Figure 6 Pressure evolution at x = 0.075 m for F = 0.001 *(a)* and F = 0 *(b)*: bundle (solid), hole (○). Trajectory in the p-T plane at x = 0.075 m for F = 0.001 *(c)* and F = 0 *(d)*: bundle (solid) and hole (o) helium. The dashed line represents the saturation curve

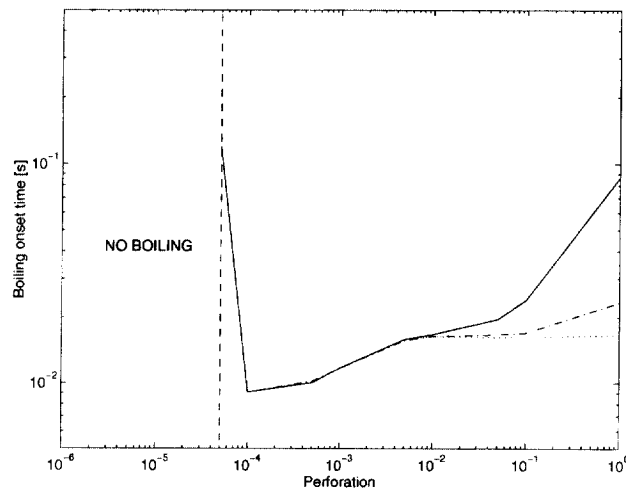

Figure 7 Boiling onset time vs. perforation with H_{nowall} = 1 (dotted), H_{nowall} = 10 (dash-dotted) and H_{nowall} = 100 (solid). Input power = 45936 W/m at t = 0

between hole and bundle. Hence we have considered in addition a parametric variation in the range 1–100 of H_{nowall} – the arbitrary multiplier in the heat transfer coefficient through the perforation between hole and bundle used in Mithrandir + . Variations in this range do not significantly affect the conclusions above on τ_B.

The predicted non-monotonic behavior of the boiling onset time τ_B in *Figure 7* can be at least qualitatively understood. At very low perforations the pressure in the bundle increases relatively quickly, because of the small exhaust to the hole. At very large perforations (and large H_{nowall}) the temperature in the bundle increases relatively slowly because of the excellent coupling to the hole. Both effects lead to a longer τ_B.

Boiling appears in the simulations rather independently of changes in other input parameters (not shown here). At lower input power, ~ 20 kW/m at t = 0, boiling sets on also for vanishing F. With 8kA current, and/or with only, e.g., 10% of the input power going directly into the strands and 90% into the jacket[7], it occurs on a similar time scale as above.

Owing to the fact that in our simulations boiling onset is insensitive to several parameters, we believe that, in the experiment, He boiled in the initial heated zone. Although no dedicated diagnostic was available in the experiment, there seems to be evidence of boiling at some point during the quench[15].

Finally, other simulations we performed (not shown here) on the parametric influence of the G-M heat conduction show that its effect on quench characteristics is rather small, as opposite to the thermal-hydraulic experiments discussed above. This is related to the fact that in the case at hand the helium behind or near the quench front spends just a short time as HeII, and then quickly becomes HeI.

Qualitative longer-term evolution of the quench

Notwithstanding the limitations in the validity of the model after boiling onset mentioned above, it is interesting to at least qualitatively extend the analysis to the longer-term propagation of the quench. This allows a preliminary comparison with measured quantities, i.e., the resistive voltage drop ΔV across the normal zone (see *Figure 8*a) and the quench front propagation speed V_q (see *Figure 8*b).

When comparing our predictions for nominal F with the experiment, we notice that ΔV is overestimated. On the other hand, the computed V_q is about half of the experimental value, which is of the order of 2.5 m/s for the 6kA quench[16]. Notice that, in the experiment, V_q was roughly estimated as an average over the first turn (~ 1 m length), which goes normal in approximately 400 ms. In the case of nominal perforation the helium speed in the bundle (not shown), computed at the quench front, turns out to be smaller than V_q, indicating that the quench is not propagated by convection in the bundle helium only. On the contrary, in the case of smaller to vanishing F (see below) the quench appears to be mainly pressure driven, with quench propagation speed smaller than, but of the same order of, the flow speed in the bundle.

In order to qualitatively explain the disagreement in the resistive voltage drop we note firstly that the computed temperature of the heated region rises quickly to extremely large values, of the order of 1000 K at t = 2 s in the nominal case. Typical temperature gradients of the order of 100 K/m develop between the initial normal zone and the yet superconducting region. Because of the strong non-linearity in the copper resistivity, the voltage drop is largely determined by the high temperature portion of the normal region, i.e., a length of the order of the initial normal zone. We conclude that the overestimated voltage drop indicates that the simulated conductor temperature in the initial normal zone is too high.

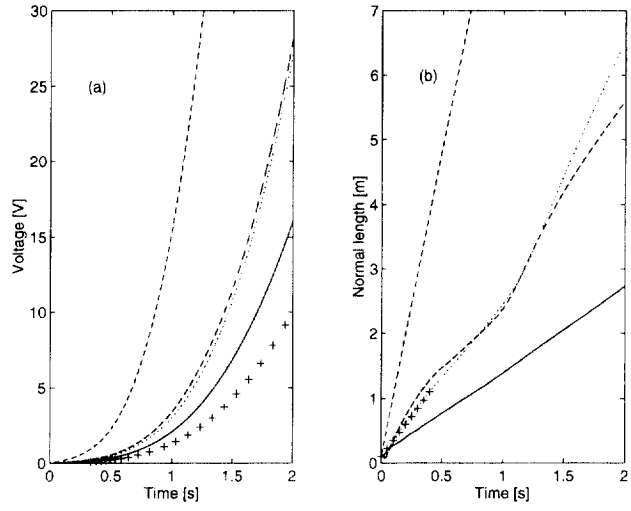

Figure 8 Full-coil voltage *(a)* and normal zone length *(b)* in the case of I = 6 kA, input power = 45936 W/m, with H_{nowall} = 1: F = 0.001 (solid), F = 0.00001 (dashed), F = 0 (dotted). The dash-dotted curve simulates 'dry quench' conditions (see text). Experimental points (' + '): the values of normal zone length are based on the single measurement available at 400 ms, when the first turn (~ 1 m length) went normal, assuming constant propagation speed of the quench

This can be qualitatively explained by the concurrence of several limitations of the model presented here. Firstly, the neglect of the details of the two-phase transition results in an underestimate of the heat transfer coefficient and of the effective heat sink provided by the helium (constant T during phase transition). Secondly, the model assumes adiabatic conditions at the outer perimeter of the conductor, certainly not appropriate for such a large temperature excursion and gradient build-up. Proper accounting for both phenomena would tend to decrease the final conductor temperature in the hot spot, and thus the normal voltage.

Regarding the discrepancy on the normal zone propagation speed, it is more difficult to draw clear conclusions. The quench propagation had been expected to be faster in the design phase of the experiment, and the coil was not extensively instrumented close to the initial normal zone. This prevented a precise determination of the evolution of the normal zone in the time range of the runs. In the initial phase of quench, for which the estimated experimental velocity is available, several phenomena could severely affect the propagation. In particular the heat transfer coefficient and the temperature gradient at the front are rather uncertain and this could explain in part the large discrepancy observed. Additionally, and possibly more important, it should be emphasized that the role of the hole in the quench propagation in perforated two-channel CICCs is not very clear at present, not even for HeI. This will be the subject of a separate investigation to be presented elsewhere by the authors.

We now turn to the discussion of parametric effects of the perforated fraction F. We consider only values of F below the nominal one (0.001), which already is very

small. Therefore, it is to be expected that the major influence of F will be on the helium pressure, while the helium temperature will be less affected.

The increase in ΔV when F decreases (*Figure* 8a) is directly related to a correspondingly longer normal zone as discussed below, whereas the conductor temperature is not very affected.

An increase in V_q is observed in the simulation when F decreases (*Figure* 8b), in qualitative agreement with the prediction of simpler models[17]. The dependence of V_q on F is partly due to a larger pressure (gradient) driving the quench when F decreases. In all cases the quench propagates at an approximately constant speed in the simulation. We notice finally that the agreement with the experiment, which obtains in the case of very small to vanishing F (see *Figure* 8b) should be considered as fortuitous.

We also simulated the same case in the limit of a 'dry' quench, assuming vanishing heat transfer coefficients. The computed V_q turned out to be about 10 m/s (*Figure* 8b), which seems to rule out the sudden helium expulsion into the hole as an explanation for dry quench propagation in QUIPS.

In view of the several uncertainties in this problem, and comparing with the relative roughness of previous estimates[17], we consider the present agreement between simulations and experiment to be reasonable.

Conclusions

Mithrandir, a 1-D two-channel model for the analysis of thermal-hydraulic transients in CICCs, has been extended to helium II.

The model for the helium in each channel (cable bundle or hole) can be justified under reasonable approximations starting from the classical two-fluid model of Landau, and reduces to the addition of Gorter-Mellink heat transport in the pressure and temperature equations. The thermal-physical properties have been rewritten in the form of tables to reduce the computational burden.

The code has been validated showing good agreement with data from a thermal-hydraulic experiment in HeII. In the same case numerical convergence has been demonstrated.

Quench initiation and propagation in the QUIPS experiment has been modeled. Boiling is predicted to occur, in agreement with the experiment, but this limits the applicability of the model, which presently cannot treat the liquid-vapor region. Within this restriction, a qualitative agreement with the measured values of resistive voltage and quench propagation speed is obtained.

Acknowledgements

We wish to thank C.A. Luongo and J.R. Miller for providing information on QUIPS. Constructive criticism by one of the referees led to an improvement of the last section of the paper and is gratefully acknowledged.

References

1. Zanino, R., DePalo, S. and Bottura, L., *J. Fus. Energy*, 1995, **14**, 25.
2. Luongo, C., Loyd, R.J. and Peck, S.D., *IEEE Trans. Appl. Supercond.*, 1993, **3**, 332.
3. Miller, J.R. and Williams, J.E.C., *IEEE Trans. Mag.*, 1994, **25**, 1563.
4. Bottura, L., *J. Comput. Phys.*, 1996, **125**, 26.
5. Zanino, R., Bottura, L. and Marinucci, C., *IEEE Trans. Appl. Supercond.*, 1997, **7**, 493.
6. Zanino, R., Bottura, L. and Marinucci, C. to appear in *Adv. Cryo. Eng.* **43**
7. DePalo, S., Marinucci, C. and Zanino, R. to appear in *Adv. Cryo. Eng.* **43**
8. Van Sciver, S.W., *Helium Cryogenics* Plenum Press, New York 1986
9. Kitamura, T., et al., *Cryogenics*, 1997, **37**, 1.
10. Gorbounov, M.B., et al., *Adv. Cryo. Eng.*, 1996, **41**, 335.
11. Cryodata Inc., User's Guide to HEPAK, Version 3.30, October 1994.
12. Srinivasan, R. and Hofmann, A., *Cryogenics*, 1985, **25(641)**, 657.
13. Kashani, A., Van Sciver, S.W. and Strikwerda, J.C., *Num. Heat Transf. A*, 1989, **16**, 213.
14. Luongo, C.A., *J. Fus. Energy*, 1995, **14**, 103.
15. Miller, J.R. Private communication 1997.
16. Luongo, C.A., Chang, C.-L. and Partain, K.D., *IEEE Trans. Mag.*, 1994, **30**, 2569.
17. Luongo, C.A., et al., *Cryogenics ICEC Supplement*, 1994, **34**, 611.